(Received 30 September 2025, Accepted 26 November 2025, Scheduled 2 December 2025)

Laser-Tracking-Modulated Microwave Temporal Metasurfaces for Mobile Hybrid Wireless Communications

Sheng Yuan[1,#], Zhi Zhou Ding[1,#], Xin Ge Zhang[1,*], Dong Jie Wang[1], Jian Kai Sun[1], and Wei Xiang Jiang[1,2,*]

[1] *State Key Laboratory of Millimeter Waves, School of Information Science and Engineering Southeast University, Nanjing 210096, China*
[2] *Purple Mountain Laboratories, Nanjing 211111, China*

ABSTRACT: Temporal metasurfaces offer a promising platform for new-architecture wireless communications by enabling fast modulation of both electromagnetic waves and digital information. Optical control of these metasurfaces is particularly attractive as it establishes a direct physical bridge between optical and microwave signals, forming the foundation for optoelectronic hybrid communication systems. However, existing schemes are confined to static pre-alignment of the laser beam with the metasurface, lacking real-time spatial alignment capability essential for real-world mobile applications. Here, we propose and realize a mobile hybrid wireless communication system based on the designed laser-tracking-modulated microwave temporal metasurface. This communication system is constructed by integrating a photodiode-based microwave temporal metasurface, a vision-assisted laser-tracking transmitter, and a microwave receiver, enabling direct laser-to-microwave signal conversion sustained by dynamic alignment. Experimental results demonstrate that the system successfully maintains a stable hybrid communication link while the laser transmitter is in motion. This work provides a viable strategy for establishing stable hybrid wireless links for moving platforms and drones in high-mobility scenarios.

1. INTRODUCTION

Temporal metasurfaces represent a significant advancement in electromagnetic (EM) wave manipulation, distinguished by their ability to modulate rapidly the phase or amplitude of elements through predefined time-varying control signals [1–4]. By breaking the static constraint of traditional metamaterials, this unique time-domain modulation capability transcends the inherent limitations of spatial-only wave control, unlocking a suite of unprecedented functionalities, including precise harmonic synthesis [5–8], on-demand frequency conversion [9–12], and direct physical-layer information processing [13–24]. Recently, temporal metasurfaces have emerged as a transformative platform for pioneering new-architecture wireless systems, including simplified transmitters that operate without traditional mixing stages and real-time smart systems [25–28]. Therefore, it lays the foundation for intelligent EM environments, holding the potential to redefine wireless architectures for 6G and beyond [29–31].

The convergence of optical and microwave wireless technologies promises to unlock unprecedented capabilities in future communication networks [32, 33]. Optical control of EM temporal metasurfaces presents a particularly compelling direction for integrating optical and microwave technologies [15–24, 34, 35]. Such integration leverages the complementary strengths of optical signals such as high directivity, security, and bandwidth, with the broad coverage of microwaves, enabling hybrid systems at the physical layer [15–24]. Recently, several optically-controlled EM metasurfaces have been realized, demonstrating functionalities ranging from spatial beam shaping [15, 16] and free-space light-to-microwave signal transmission [17] to bidirectional microwave-optical interconversion [24]. Despite these advancements, a critical limitation remains as all previous systems operate under a spatially-fixed configuration where the light source and the metasurface require meticulous pre-alignment and maintain a stationary relative position. This inability to accommodate relative motion is the fundamental obstacle preventing deployment in real-world mobile applications, such as communications with unmanned aerial vehicles or mobile internet of things (IoTs) nodes, where continuous dynamic alignment is essential.

Here, we break this limitation by introducing a laser-tracking-modulated microwave temporal metasurface for mobile hybrid wireless communication. Unlike previous spatially-fixed systems, our light control platform integrates an intelligent vision-assisted laser tracking device comprising a camera, a high-precision motor, and AI-based algorithms to achieve real-time spatial alignment between a moving laser source and the metasurface. The temporal metasurface is realized by incorporating photodiodes onto microwave resonant structure, leveraging the photoconductive-capacitance effect to convert directly the tracked laser signal into modulated microwaves at the physical layer. This integrated design enables sustained laser-to-microwave conversion under mobility. As a demonstration, we construct a metasurface-enabled system prototype, and measured results validate stable data

* Corresponding authors: Xin Ge Zhang (xingezhang@seu.edu.cn); Wei Xiang Jiang (wxjiang81@seu.edu.cn).
# These authors contributed equally.

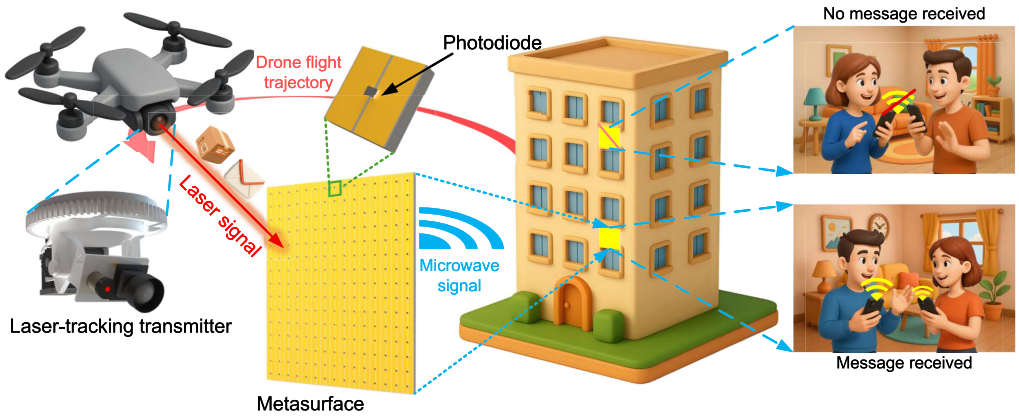

FIGURE 1. Laser-tracking-modulated microwave temporal metasurface for mobile hybrid wireless communication and its potential application scenarios.

transmission with accurate real-time tracking in dynamic scenarios, thereby establishing a viable pathway for practical mobile hybrid wireless communications.

2. RESULTS

We design a laser-tracking-modulated microwave temporal metasurface hybrid communication system for directional and confidential data transmission. To illustrate this concept, a representative potential application scenario is depicted in Figure 1. The system comprises two main components: a mobile laser-tracking transmitter mounted on an unmanned aerial vehicle and a fixed, optically-controlled microwave metasurface, typically installed on a wall. During operation, the compact laser-tracking transmitter identifies automatically the location of the metasurface and illuminates precisely it with a laser beam carrying encoded information. Each meta-element of the metasurface incorporates a microwave resonant structure integrated with photodiode. Utilizing the photoelectric effect, the meta-element modulates the incoming laser signal into the microwave domain, thereby achieving real-time optical-to-microwave signal conversion. The converted data are then transmitted to authorized indoor users through microwave signals. Due to the highly directional laser illumination and the spatial selectivity of the optically-controlled metasurface, the system inherently provides enhanced directional privacy and resistance to interception. Unauthorized users who lack access to the laser-illuminated metasurface cannot receive or decode the transmitted information, ensuring confidentiality through spatial selectivity.

2.1. Optically-Controlled Microwave Metasurface Design

To achieve efficient conversion from laser to microwave signals, the metasurface needs to response to both optical and microwave fields, while operating without a direct-current (DC) power supply to minimize system complexity. For microwave dynamic modulation, a dielectric substrate combined with carefully-designed metallic patterns forms a resonant structure highly sensitive to microwave fields. This resonator is engineered to exhibit a strong response to impedance variations, allowing external optical signals to effectively modulate the microwave reflection. To further achieve the optical control of the microwave metasurface, we integrate photosensitive components such as photodiodes into the microwave resonator. Under optical illumination, the junction capacitance will be changed, thus tuning the microwave reflection of the metasurface.

Guided by this principle, we design and fabricate an optically-controlled microwave metasurface without any DC power connection, as shown in Figure 2. The designed meta-element has a square periodicity of $p = 15\,\text{mm}$, as illustrated in Figure 2(a). The metallic pattern functions as a microwave resonator, with a photodiode (model S13773) bridging two segments of the structure. Key dimensions include $w_1 = 14.6\,\text{mm}$ and $w_2 = 0.2\,\text{mm}$. Under laser illumination, photogenerated carriers alter the depletion region width of the PN junction of the photodiode, modulating its junction capacitance. Since the photodiode is integrated into the microwave resonant structure, this capacitance change directly shifts the EM response of the meta-element. When a microwave signal illuminates the temporal meta-element, the laser-induced capacitance variation modulates the reflection amplitude, thereby encoding the optical input onto the reflected microwave signal.

To quantify how the photodiode's junction-capacitance variation influences the metasurface's reflection coefficient and resonance frequency, we conduct a simulation that integrates an equivalent circuit model with the experimentally measured S-parameters of the photodiode (see **Supporting Information Note 1**). The resulting response is shown in Figure 2(b), which presents the simulated reflection amplitude of the optically-controlled meta-element under laser-on and laser-off conditions. When the laser source is off, the photodiode remains dark and the meta-element resonates near 4.2 GHz. When the laser is turned on, the photodiode is illuminated and its photocapacitive response changes the equivalent capacitance, shifting the resonance to about 3.8 GHz. By cycling the laser between these two states modulates the amplitude of the reflected microwave and realizes effectively on-off keying (OOK) of the microwave signal. Furthermore, the increased junction capacitance under

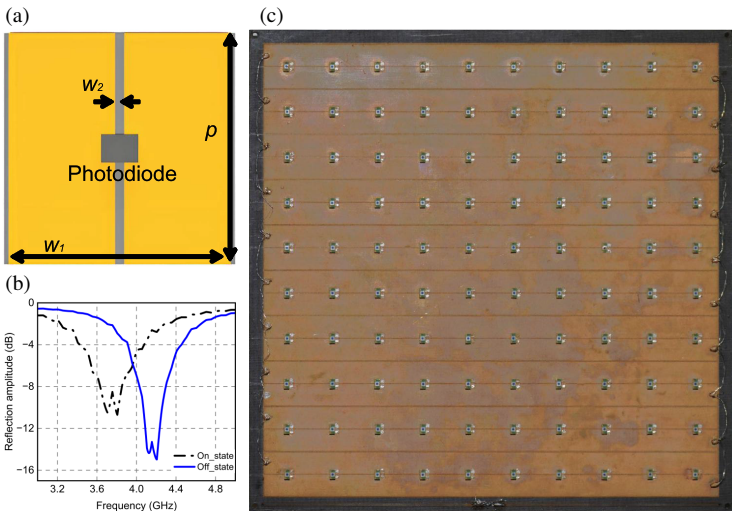

FIGURE 2. Optically-controlled microwave metasurface. (a) Schematic of the photodiode-based meta-element. (b) Simulated reflection amplitude of the meta-element under two different laser illuminating states. (c) Photograph of the fabricated optically-controlled microwave metasurface.

illumination shifts the resonance [20], confirming the photodiode's function as an optically-controlled capacitor.

As a demonstration, a metasurface prototype containing 10×10 meta-elements is fabricated, as shown in Figure 2(c), and the detailed electrical connections of the meta-elements are described in **Supporting Information Note 2**. This design ensures that illuminating even a single photodiode can trigger a capacitance response across the entire array, allowing full metasurface modulation with a single laser beam. This approach significantly reduces the required number of light sources while maintaining high modulation performance.

2.2. Implementation of Laser-Tracking Transmitter

To enable laser-to-microwave signal conversion in optically-controlled microwave temporal metasurface applications, the laser beam should be projected accurately onto the photodiodes within the target meta-elements. Traditional static illumination approaches are inadequate for dynamic scenarios, necessitating the development of a laser-tracking platform capable of real-time target localization and continuous alignment to ensure reliable metasurface operation. Commonly employed laser-tracking techniques include galvanometer scanners, micro-electro-mechanical systems micromirrors, and gimbal mechanisms [36, 37]. The first two options provide advantages such as rapid response times and compact form factors, making them suitable for high-speed scanning over limited angular ranges. However, their usefulness is constrained by restricted optical apertures and narrow scanning angles, rendering them impractical for wide-area applications. In contrast, gimbal-based systems deliver extensive angular coverage and high load capacity. Their ability to maintain stable co-alignment of a laser and camera makes them particularly well-suited for long-distance and wide-field tracking tasks, such as those encountered in unmanned aerial vehicle communications, vehicular laser alignment, and low-altitude economy applications.

We develop a low-cost laser-tracking transmitter based on a gimbal structure, which primarily consists of a target perception and laser emission module (Figure 3(a)) and a control and processing module (Figure 3(b)). As shown in Figure 3(a), the perception and emission module integrates two stepper motors and each paired with a high-precision 3D-printed reduction gear train, a varifocal camera, and a laser source. The stepper motors drive the pitch and yaw axes, with the gear trains achieving an angular resolution of 0.014° per axis. The camera supports a maximum resolution of 3840×2160 and provides a focal length range of 3.41–10.33 mm. The laser source delivers an output power of up to 100 mW with an adjustable spot size. The control and processing module (Figure 3(b)) includes an embedded Jetson Orin Nano board and a high-speed current driver. The Jetson board captures images via a universal serial bus (USB) port, controls the stepper motors, and outputs laser modulation signals through its input/output (I/O) ports, while the current driver amplifies these signals to drive the laser diode.

The operational workflow of the laser-tracking transmitter is illustrated in Figures 3(c)–(g). When image data are acquired by the perception module, the embedded Jetson processor first employs a custom YOLO-based detection algorithm to identify whether a metasurface target is present in the field of view. Upon successful recognition, the control module drives the gimbal mechanism to perform precise attitude adjustment, aligning the optical axis and directing the laser beam toward the target photodiode, as shown in Figure 3(c). To enhance detection reliability, the training dataset incorporates not only annotated images of the optically-controlled microwave temporal metasurface and fiducial-marked photodiodes but also diverse background scenes, effectively suppressing false alarms and improving target-background discriminability. The laser modulation process is detailed in Figure 3(d). Taking image transmission as an example, the red-green-blue (RGB) pixel data are first converted into a binary sequence, which is then delivered to the current driver to modulate the laser diode. The

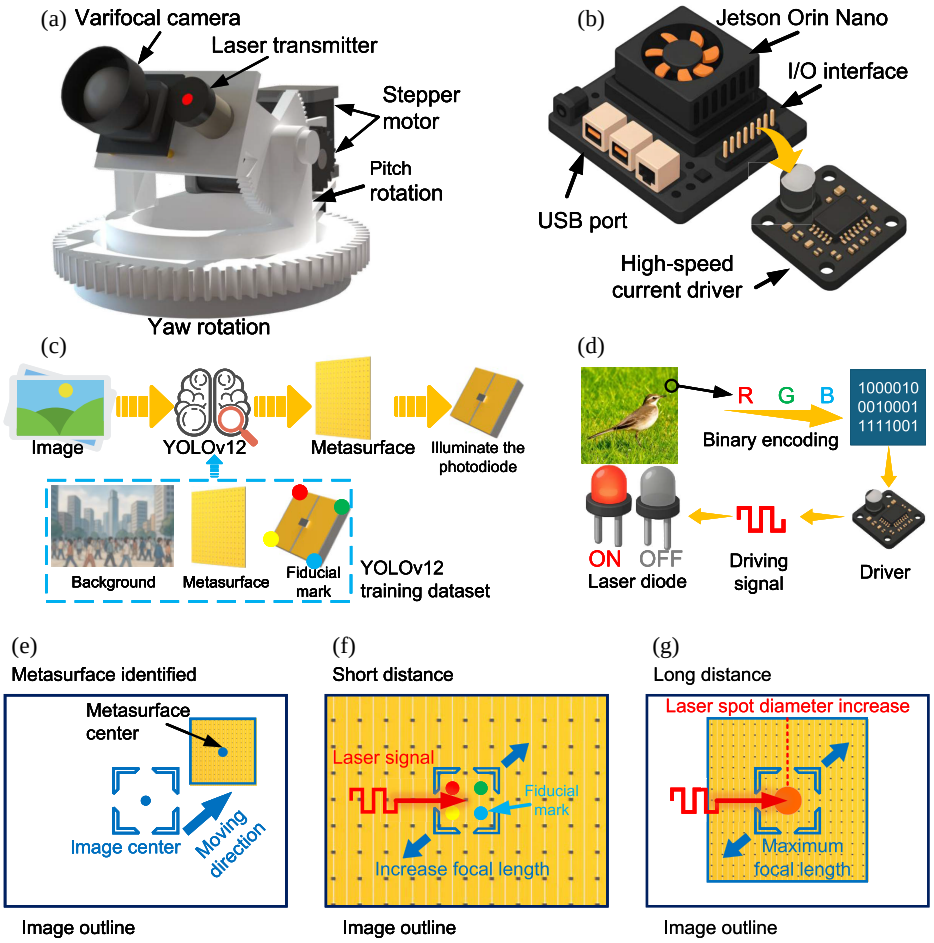

FIGURE 3. Architecture and operating principles of the laser tracking transmitter. (a) Target-tracking and laser-emission module. (b) Information processing and control module. (c) The workflow of laser tracking transmitter. (d) Laser data modulation principle. (e) Metasurface tracking and motion control. (f) Short-distance tracking and laser alignment. (g) Long-distance tracking and laser alignment.

diode emits laser and remains off for implementing on-off keying (OOK) modulation for the intensity-carried laser signal.

The alignment and tracking strategy of the laser-tracking transmitter is detailed in Figure 3(e). After the metasurface is identified successfully, the laser-tracking transmitter calculates the positional offset between the target center and the image center, then drives the gimbal to rotate until both centers are aligned. The stepper motors, equipped with integrated proportional-integral-derivative (PID) controllers and high-resolution encoders, support a maximum rotational speed of 3000 rpm, enabling fast and stable pointing control. At short operating distances, the highly focused laser spot tends to become misaligned with the photodiode, as shown in Figure 3(f). To enhance alignment precision, the system increases the camera focal length to clearly resolve the fiducial marker. This marker consists of four color-coded labels distributed in a square layout with a center spacing of 20 mm, which not only assist in locating the photodiode but also allow estimation of the target distance. Based on the estimated distance, the laser-tracking transmitter further optimizes the gimbal pointing angle to ensure the laser spot accurately illuminates the photodiode area. At long operating distances, where the fiducial marker becomes undetectable even at the camera's maximum focal length, alignment can still be achieved by overlapping the laser spot with the center of the metasurface, since the laser beam diameter increases with distance (Figure 3(g)). While this slightly reduces the optical power density on the photodiode, it effectively preserves the stability of the communication link.

To achieve robust target recognition and tracking, we train a YOLOv12 [38, 39] model on a custom dataset comprising three categories: 100 metasurface samples captured from varying distances and perspectives, 100 images of photodiodes with the fiducial marker, and 50 background images containing no targets. The detailed description of the YOLOv12 model architecture and training parameters used is provided in **Supporting Information Note 3**, and the training performance metrics are summarized in Figures 4(a), (b). Here, each epoch corresponds to a full pass through the training data, while box_loss, cls_loss, and dfl_loss denote the loss terms for bounding-box regression, object classification, and distribution-based localization, respectively. All three losses decrease rapidly and converge within the first 10–20 epochs, indicating effective feature learning in both localization and classification tasks. During evaluation, Precision (P) and Recall (R) reflecting detection accuracy and completeness, respectively and both approach 1.0, demonstrating minimal false positives and false negatives. The mean

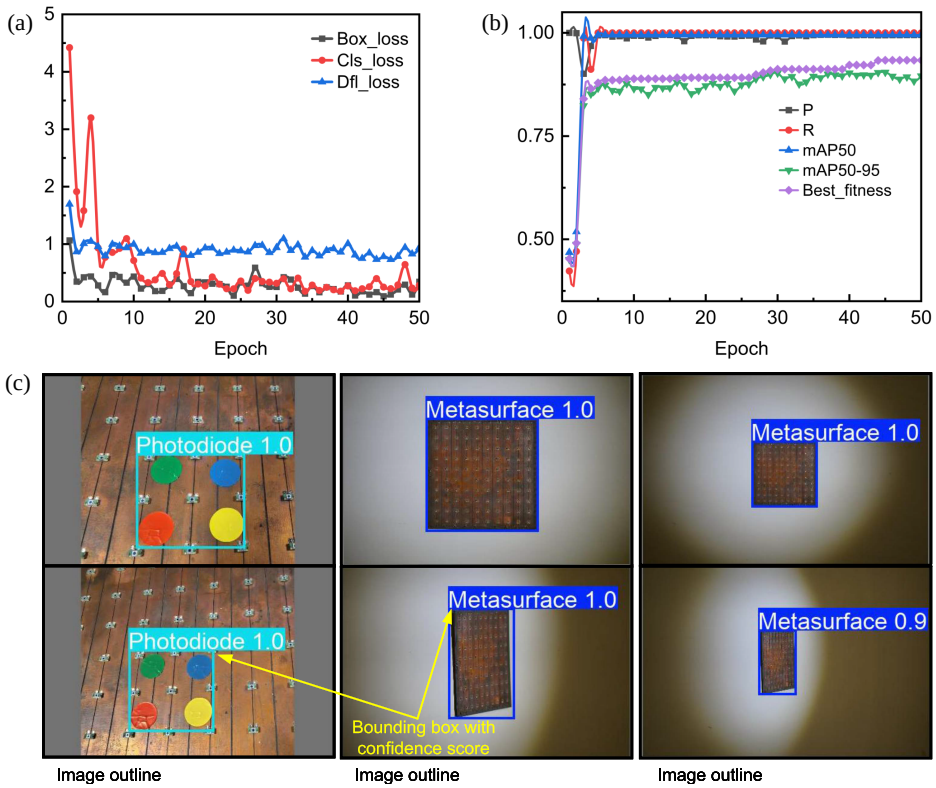

FIGURE 4. YOLO model performance and simulated test results. (a) Dynamic changes of training parameters (box_loss, cls_loss, and dfl_loss) during the training process. (b) Dynamic changes of training parameters (P, R, mAP50, mAP50-95, and best_fitness) during the training process. (c) Recognition performance of the YOLO model under simulated distances and incidence angles.

Average Precision (mAP) under Intersection over Union (IoU) thresholds of 0.5 (mAP50) and 0.5–0.95 (mAP50–95) further confirms strong detection performance, with mAP50 nearing perfection and mAP50–95 exceeding 0.89, underscoring the model's rapid and stable convergence. The composite metric best_fitness, derived as a weighted combination of key criteria, was used to select the final model, which achieved a recognition accuracy of approximately 94% in testing. To verify real-world applicability, the model is evaluated on a validation set, where it consistently maintains reliable detection across targets of diverse sizes and viewing angles, as shown in Figure 4(c).

2.3. Mobile Hybrid Wireless Communication System

To validate the feasibility and stability of the proposed scheme, we construct an experimental system for laser-tracking-modulated microwave temporal metasurface hybrid communication. A schematic diagram of the hybrid communication system is shown in Figure 5(a). In this system, the image is first encoded into laser signals via OOK modulation. When the laser illumination reaches the photodiode-integrated metasurface, the optical signal induces a junction-capacitance change that modulates the microwave reflection. However, due to the significantly increased equivalent capacitance caused by the large number of parallelly connected meta-elements, combined with the broad spectral components required by OOK modulation, the overall temporal response of the photodiode array becomes constrained. As a result, the achievable switching speed of the metasurface is around 100 kHz. After target search and beam alignment by the vision-assisted laser-tracking transmitter, the modulated laser is directed onto the photodiodes integrated in the microwave metasurface. Relying on the photoelectric effect, the photodiodes convert variations in optical intensity into junction capacitance changes, thereby modulating the reflected microwave amplitude of the metasurface, thus generating the binary amplitude-shift keying (BASK) microwave signal. The received BASK microwave signal is subsequently demodulated to reconstruct the original image data.

A photograph of the constructed mobile hybrid wireless communication system is presented in Figure 5(b), in which the microwave transceiver (transmitter and receiver) is adopted to realize microwave transmission and demodulation in our experiments. The horn antennas are positioned 1 m away from the metasurface, with the transmitting antenna and receiving antenna symmetrically placed on either side of the metasurface. The hardware implementation of the laser-tracking transmitter is illustrated in Figures 5(c), (d). The laser-tracking transmitter is mounted on a motorized sliding rail to simulate a mobile deployment scenario. The arrangement of the fiducial marker, used to indicate the central photodiode on the metasurface, is displayed in Figure 5(e). By adjusting the distance between Desk A and Desk B in the communication process, the separation between the optically-controlled metasurface and the

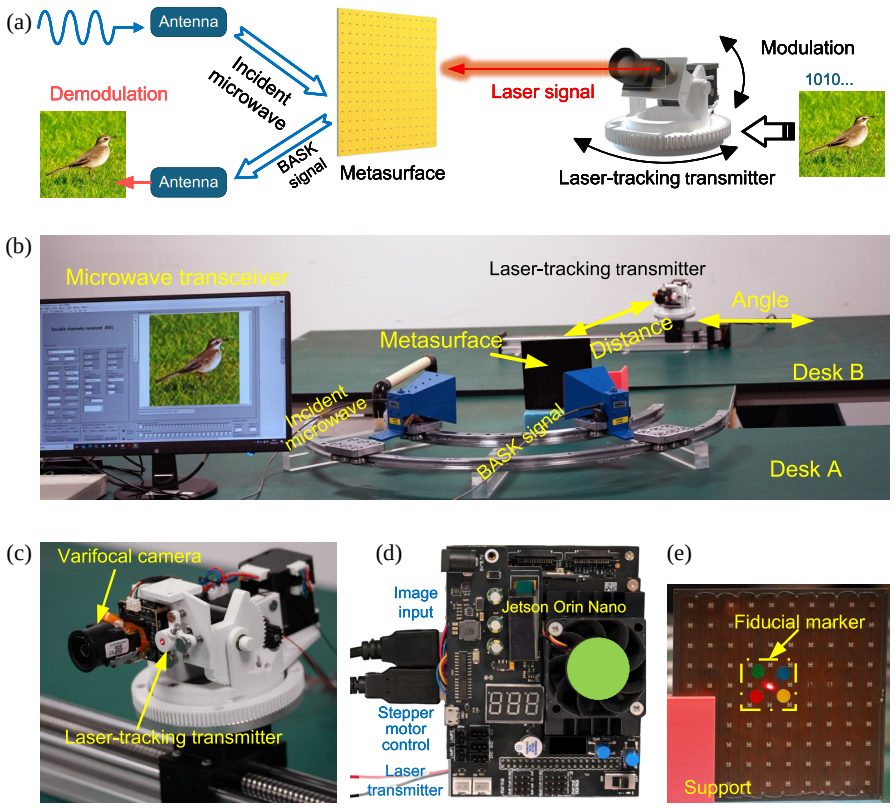

FIGURE 5. Schematic and physical setup of the mobile hybrid wireless communication experiment. (a) Schematic of the mobile hybrid communication system. (b) Photograph of the implemented mobile hybrid communication system. (c) Photograph of the target-tracking and laser-emission module. (d) Photograph of the information processing and control module. (e) Photograph of the color markers on the metasurface.

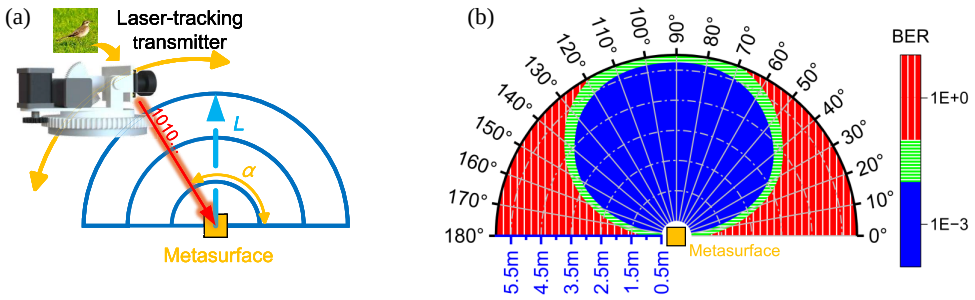

FIGURE 6. Performance evaluation of the mobile hybrid wireless communication system. (a) Schematic of the measurement principle for the maximum stable communication distance. (b) Measured BER results under incremental incident angles and transmission distances.

vision-assisted laser-tracking transmitter can be varied. Simultaneously, the motion of the sliding rail enables dynamic control of the incident angle between the laser transmitter and the metasurface normal.

To evaluate the communication stability of the laser-tracking hybrid wireless communication system, a comprehensive test is conducted with the metasurface as the center of an arc of radius L, where α denotes the angle between the laser-tracking transmitter's optical axis and the metasurface plane, as shown in Figure 6(a). In our demonstration system, digital image data are transmitted via OOK modulation, and the bit-error rate (BER) directly reflects the end-to-end communication reliability. Therefore, BER is used as the primary quantitative metric in this work. The measured BER results under incremental variations of L (0.5 m steps) and α (10° steps) are summarized in Figure 6(b). Further analysis is provided in **Supporting Information Note 5**. Experimental results show that stable communication is maintained up to 5.5 m, with the effective angular range decreasing from about 10°–170° at 0.5 m to 60°–120° at 5.5 m. The system achieves laser alignment and stabilizes communication within 1–2 s at various angles. Furthermore, we examine the communication stability under long-distance conditions (see **Supporting Information Note 4**), with emphasis on the impacts of laser-spot expansion and positional misalignment. Additionally, we assess the performance of the YOLO model on the Jetson board (see **Supporting Information Note 6**), focusing on its training time, real-time detection accuracy, and processing latency.

3. CONCLUSION

In summary, we have demonstrated a metasurface-based mobile hybrid wireless communication system empowered by vision-assisted laser-tracking that effectively tackles the dual challenges of efficient laser-to-microwave conversion and real-time alignment in laser communication. Our design lies the heterogeneous integration of photodiodes exhibiting strong photocapacitive response with microwave resonant structures. This synergy enables direct optical-to-microwave modulation without external DC bias, significantly reducing system complexity and power consumption. To overcome the limitation of static laser alignment in conventional systems, we further developed a low-cost vision-assisted laser-tracking transmitter that combines real-time object detection with a gimbal-based steering mechanism. This integrated approach supports wide-range target search and high-precision beam alignment, ensuring sustained link stability under mobile conditions. Experimental validation confirms that the system reliably transmits laser-encoded information via microwave backscatter while maintaining robust tracking and communication performance during platform motion. With its distinctive advantages in power efficiency, directional security, and dynamic operability, the proposed architecture opens up practical pathways for wireless communication in next-generation IoTs, smart logistics, low-altitude economy, and other mobility-aware applications.

ACKNOWLEDGEMENT

This work was supported by the National Natural Science Foundation of China (U23B2015, 62201143 and 62288101), the Natural Science Foundation of Jiangsu Province (BK20212002), the Jiangsu Joint Laboratory of Multidimensional Perceptual Information Technology (BM2022017), the Jiangsu Provincial Key Research and Development Program (BG2024029), the China National Postdoctoral Program for Innovative Talents (BX2021063), and the China Postdoctoral Science Foundation (2021M700762).

REFERENCES

[1] Zhang, L., X. Q. Chen, S. Liu, Q. Zhang, J. Zhao, J. Y. Dai, G. D. Bai, X. Wan, Q. Cheng, G. Castaldi, V. Galdi, and T. J. Cui, "Space-time-coding digital metasurfaces," *Nature Communications*, Vol. 9, No. 1, 4334, 2018.

[2] Taravati, S. and G. V. Eleftheriades, "Microwave space-time-modulated metasurfaces," *ACS Photonics*, Vol. 9, No. 2, 305–318, 2022.

[3] Guo, X., Y. Ding, Y. Duan, and X. Ni, "Nonreciprocal metasurface with space-time phase modulation," *Light: Science & Applications*, Vol. 8, No. 1, 123, 2019.

[4] Karl, N., P. P. Vabishchevich, M. R. Shcherbakov, S. Liu, M. B. Sinclair, G. Shvets, and I. Brener, "Frequency conversion in a time-variant dielectric metasurface," *Nano Letters*, Vol. 20, No. 10, 7052–7058, 2020.

[5] Ke, J. C., J. Y. Dai, J. W. Zhang, Z. Chen, M. Z. Chen, Y. Lu, L. Zhang, L. Wang, Q. Y. Zhou, L. Li, *et al.*, "Frequency-modulated continuous waves controlled by space-time-coding metasurface with nonlinearly periodic phases," *Light: Science & Applications*, Vol. 11, No. 1, 273, 2022.

[6] Wang, X., M. S. Mirmoosa, V. S. Asadchy, C. Rockstuhl, S. Fan, and S. A. Tretyakov, "Metasurface-based realization of photonic time crystals," *Science Advances*, Vol. 9, No. 14, eadg7541, 2023.

[7] Wu, G.-B., J. Y. Dai, K. M. Shum, K. F. Chan, Q. Cheng, T. J. Cui, and C. H. Chan, "A universal metasurface antenna to manipulate all fundamental characteristics of electromagnetic waves," *Nature Communications*, Vol. 14, No. 1, 5155, 2023.

[8] Zhang, X. G., Y. L. Sun, Q. Yu, Q. Cheng, W. X. Jiang, C.-W. Qiu, and T. J. Cui, "Smart doppler cloak operating in broad band and full polarizations," *Advanced Materials*, Vol. 33, No. 17, 2007966, 2021.

[9] Takeshita, H., A. A. Fathnan, D. Nita, A. Nagata, S. Sugiura, and H. Wakatsuchi, "Frequency-hopping wave engineering with metasurfaces," *Nature Communications*, Vol. 15, No. 1, 196, 2024.

[10] Wu, H., X. X. Gao, L. Zhang, G. D. Bai, Q. Cheng, L. Li, and T. J. Cui, "Harmonic information transitions of spatiotemporal metasurfaces," *Light: Science & Applications*, Vol. 9, No. 1, 198, 2020.

[11] Stefanini, L., D. Ramaccia, M. Barbuto, M. Longhi, A. Monti, S. Vellucci, A. Toscano, A. Alu, V. Galdi, and F. Bilotti, "Time-varying metasurfaces for efficient surface-wave coupling to radiation and frequency conversion," *Laser & Photonics Reviews*, Vol. 18, No. 12, 2400315, 2024.

[12] Wang, X., V. S. Asadchy, S. Fan, and S. A. Tretyakov, "Space-time metasurfaces for power combining of waves," *ACS Photonics*, Vol. 8, No. 10, 3034–3041, 2021.

[13] Shadrivov, I. V., P. V. Kapitanova, S. I. Maslovski, and Y. S. Kivshar, "Metamaterials controlled with light," *Physical Review Letters*, Vol. 109, No. 8, 083902, 2012.

[14] Pors, A., M. G. Nielsen, and S. I. Bozhevolnyi, "Analog computing using reflective plasmonic metasurfaces," *Nano Letters*, Vol. 15, No. 1, 791–797, 2015.

[15] Zhang, X. G., W. X. Tang, W. X. Jiang, G. D. Bai, J. Tang, L. Bai, C.-W. Qiu, and T. J. Cui, "Light-controllable digital coding metasurfaces," *Advanced Science*, Vol. 5, No. 11, 1801028, 2018.

[16] Zhang, X. G., W. X. Jiang, H. L. Jiang, Q. Wang, H. W. Tian, L. Bai, Z. J. Luo, S. Sun, Y. Luo, C.-W. Qiu, and T. J. Cui, "An optically driven digital metasurface for programming electromagnetic functions," *Nature Electronics*, Vol. 3, No. 3, 165–171, 2020.

[17] Zhang, X. G., Y. L. Sun, B. Zhu, W. X. Jiang, Z. Zhang, and T. J. Cui, "Light-controllable time-domain digital coding metasurfaces," *Advanced Photonics*, Vol. 4, No. 2, 025001, 2022.

[18] Sun, Y. L., X. G. Zhang, Z. Huang, H. W. Tian, T. J. Cui, and W. X. Jiang, "Intelligent transmissive microwave metasurface with optical sensing and transparency," *Research*, Vol. 7, 0514, 2024.

[19] Sayanskiy, A., A. Belov, R. Yafasov, A. Lyulyakin, A. Sherstobitov, S. Glybovski, and V. Lyashev, "A 2D-programmable and scalable reconfigurable intelligent surface remotely controlled via digital infrared code," *IEEE Transactions on Antennas and Propagation*, Vol. 71, No. 1, 570–580, 2023.

[20] Zhang, X. G., Y. L. Sun, B. Zhu, J. Wang, T. Zhao, W. X. Jiang, Z. Huang, Z. Zhang, and T. J. Cui, "Optoelectronic metasurface for free-space optical-microwave interactions," *ACS Applied Materials & Interfaces*, Vol. 15, No. 18, 22 744–22 751, 2023.

[21] Hu, S., C. Wang, S. Du, Z. Han, N. Hu, and C. Gu, "Laser-induced reconfigurable wavefront control with a structured $Ge_2Sb_2Te_5$-based metasurface," *Communications Physics*, Vol. 7, 346, 2024.

[22] Sanjari, P. and F. Aflatouni, "A reconfigurable non-linear active metasurface for coherent wave down-conversion," *Nature Communications*, Vol. 16, No. 1, 1987, 2025.

[23] Chen, B., J. Wu, W. Li, C. Zhang, K. Fan, Q. Xue, Y. Chi, Q. Wen, B. Jin, J. Chen, and P. Wu, "Programmable terahertz metamaterials with non-volatile memory," *Laser & Photonics Reviews*, Vol. 16, No. 4, 2270019, 2022.

[24] Zhang, X. G., Y. L. Sun, B. Zhu, H. W. Tian, B. Y. Wang, Z. Zhang, C.-W. Qiu, T. J. Cui, and W. X. Jiang, "Wireless microwave-to-optical conversion via programmable metasurface without DC supply," *Nature Communications*, Vol. 16, No. 1, 528, 2025.

[25] Tang, W., J. Y. Dai, M. Chen, X. Li, Q. Cheng, S. Jin, K.-K. Wong, and T. J. Cui, "Programmable metasurface-based RF chain-free 8PSK wireless transmitter," *Electronics Letters*, Vol. 55, No. 7, 417–420, 2019.

[26] Ataloglou, V. G., S. Taravati, and G. V. Eleftheriades, "Metasurfaces: Physics and applications in wireless communications," *National Science Review*, Vol. 10, No. 8, nwad164, 2023.

[27] Ke, J. C., L. Wang, M. Jiang, and Q. Wang, "Wireless communication using a radiation-type metasurface," *Micromachines*, Vol. 16, No. 8, 924, 2025.

[28] Bai, X., S. Tan, S. Mikki, E. Li, and T.-J. Cui, "Information-theoretic measures for reconfigurable metasurface-enabled direct digital modulation systems: An electromagnetic perspective," *Progress In Electromagnetics Research*, Vol. 179, 1–18, 2024.

[29] Jin, L., J. Xie, B. Pan, and G. Luo, "Generalized phase retrieval model based on physics-inspired network for holographic metasurface," *Progress In Electromagnetics Research*, Vol. 178, 103–110, 2023.

[30] Zhou, H., M. Erol-Kantarci, Y. Liu, and H. V. Poor, "A survey on model-based, heuristic, and machine learning optimization approaches in ris-aided wireless networks," *IEEE Communications Surveys & Tutorials*, Vol. 26, No. 2, 781–823, 2024.

[31] Ra'di, Y., N. Nefedkin, P. Popovski, and A. Alù, "Metasurfaces for next-generation wireless communication systems," *National Science Review*, Vol. 10, No. 8, nwad140, 2023.

[32] Tao, Z., H. Wang, H. Feng, Y. Guo, B. Shen, D. Sun, Y. Tao, C. Han, Y. He, J. E. Bowers, *et al.*, "Ultrabroadband on-chip photonics for full-spectrum wireless communications," *Nature*, Vol. 645, 80–87, 2025.

[33] Sharma, T., A. Chehri, and P. Fortier, "Review of optical and wireless backhaul networks and emerging trends of next generation 5G and 6G technologies," *Transactions on Emerging Telecommunications Technologies*, Vol. 32, No. 3, e4155, 2021.

[34] Tian, H. W., Y. L. Sun, X. G. Zhang, X. Li, Q. Zhu, C. Song, C.-W. Qiu, T. J. Cui, and W. X. Jiang, "Solar-powered light-modulated microwave programmable metasurface for sustainable wireless communications," *Nature Communications*, Vol. 16, No. 1, 2524, 2025.

[35] Jones, T. R., A. V. Kildishev, M. Segev, and D. Peroulis, "Time-reflection of microwaves by a fast optically-controlled time-boundary," *Nature Communications*, Vol. 15, No. 1, 6786, 2024.

[36] Chen, B. and H. Yu, "Visual tracking for mobile optical wireless communications," *Optics Express*, Vol. 28, No. 21, 31 119–31 126, 2020.

[37] Lee, D.-H., D.-Q. Tran, Y.-B. Kim, and S. Chakir, "A robust double active control system design for disturbance suppression of a two-axis gimbal system," *Electronics*, Vol. 9, No. 10, 1638, 2020.

[38] Yang, Z., Z. Khan, Y. Shen, and H. Liu, "GTDR-YOLOv12: Optimizing YOLO for efficient and accurate weed detection in agriculture," *Agronomy*, Vol. 15, No. 8, 1824, 2025.

[39] Ji, Y., T. Ma, H. Shen, H. Feng, Z. Zhang, D. Li, and Y. He, "Transmission line defect detection algorithm based on improved YOLOv12," *Electronics*, Vol. 14, No. 12, 2432, 2025.